

# Core-Double-Shell Fe<sub>3</sub>O<sub>4</sub>@Carbon@Poly(In<sup>III</sup>-carboxylate) Microspheres: Cycloaddition of CO<sub>2</sub> and Epoxides on Coordination Polymer Shells Constituted by Imidazolium-Derived Al<sup>III</sup>-Salen Bifunctional Catalysts

Qiao An,<sup>†</sup> Zifeng Li,<sup>†</sup> Robert Graff,<sup>‡</sup> Jia Guo,<sup>\*,†</sup> Haifeng Gao,<sup>‡</sup> and Changchun Wang<sup>†</sup>

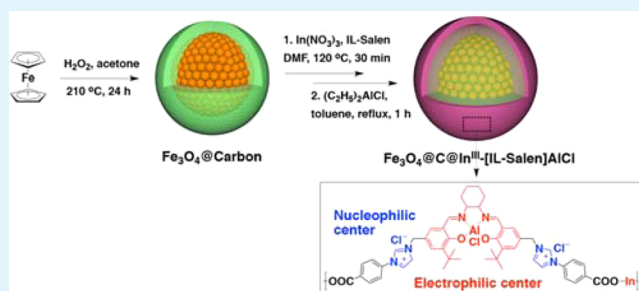
<sup>†</sup>State Key Laboratory of Molecular Engineering of Polymers, Department of Macromolecular Science, Fudan University, Shanghai 200433, People's Republic of China

<sup>‡</sup>Department of Chemistry and Biochemistry, University of Notre Dame, Notre Dame, Indiana 46556-5670, United States

## S Supporting Information

**ABSTRACT:** A hybrid microsphere Fe<sub>3</sub>O<sub>4</sub>@carbon@poly-(In<sup>III</sup>-carboxylate) consisting of a cluster of Fe<sub>3</sub>O<sub>4</sub> nanoparticles as the core, a carbon layer as the inner shell and a porous In<sup>III</sup>-carboxylate coordination polymer as the outer shell was prepared and applied as a recyclable catalyst for the cycloaddition reaction of CO<sub>2</sub> and epoxides. Construction of this hybrid microsphere was achieved in the two steps, including (1) the one-pot solvothermal synthesis of Fe<sub>3</sub>O<sub>4</sub>@C particles with the abundant carboxylic groups on the carbon surface and (2) the subsequent growth of the outer shell polymers based on the precipitation coordination polymerization. Imidazolium-substituted Salen ligands were synthesized and chelated with the In(III) ions using the terminal carboxylic groups. The coordination polymer shell was formed on the Fe<sub>3</sub>O<sub>4</sub>@C particles, and the structures including shell thickness, surface area and porosity could be varied by tuning the feeding ratios of the In(III) ions and the ligands. The optimal structure of the coordination polymers showed a shell thickness of ca. 45 nm with ~5 nm of mesopore, 174.7 m<sup>2</sup>/g of surface area and 0.2175 cm<sup>3</sup>/g of pore volume. In light of gas uptake capability, catalytic activity and magnetic susceptibility, cycloaddition of CO<sub>2</sub> with a series of epoxides were studied by using Al-complexed Fe<sub>3</sub>O<sub>4</sub>@C@In<sup>III</sup>-[IL-Salen] microspheres. The results validated that the self-supporting catalytic layer with high surface area was of remarkable advantages, which were attributed from great increment of effective active sites and combination of nucleophilic/electrophilic synergistic property and CO<sub>2</sub> uptake capability. Therefore, these hybrid microspheres provided excellent catalytic activity, prominent selectivity to cyclic carbonates and outstanding recyclability with the assistance of an applied magnetic field.

**KEYWORDS:** bifunctional catalysts, CO<sub>2</sub>, coordination polymers, cycloaddition, magnetic nanoparticles



## 1. INTRODUCTION

Because ionic liquids (ILs) have nonvolatility, excellent thermal stability, wide liquid regions, powerful solvating properties and structure tenability,<sup>1,2</sup> they have attracted significant attention as an alternative reaction medium. Also, it has been proved that ILs bear exceptionally high catalytic activity and selectivity for some important reactions such as hydrogenation of alkynes, esterification, Suzuki coupling and cycloaddition of CO<sub>2</sub> with epoxides.<sup>3</sup> However, severe issues including high viscosity, hard separation and recycling, equipment corrosion and toxicity, largely limits their applicability as homogeneous catalysts. An approach to overcome these drawbacks is the development of supported ionic liquid catalysts (SILCs) that merely require catalytic amount of IL immobilized on a solid support. They combine the distinctive characteristics of ILs such as specificity and selectivity in catalysis, uniform nature of catalytic centers and versatile designability, with important features of

heterogeneous catalysts, such as high surface area, exceptional stability, and ease of handling, separation and recycling.<sup>4,5</sup> Much work has focused on SILCs with substrates, such as silica,<sup>6,7</sup> polymers,<sup>8,9</sup> zeolites<sup>10</sup> and carbon nanotubes.<sup>11</sup> Of these, high-surface-area materials appear to be generally a better choice, allowing a high loading of ILs,<sup>12</sup> and also easily perform covalent anchoring of functional modules.<sup>13,14</sup> In comparison to homogeneous catalysis, reduced catalytic activity of immobilized ILs is found. It is thought that the adsorption of ILs into the micro/mesopores of the substrates by noncovalent or covalent interactions may be compromising their catalytic activity.<sup>5</sup> It is therefore anticipated that a desirable SILC should

Received: January 5, 2015

Accepted: February 12, 2015

Published: February 12, 2015

be designed not only to allow for affinity of ILs to the substrate, but also to maintain IL's ability to efficiently catalyze reactions.

Coordination polymer particles (CPPs), constructed by repeating metal–ligand topological structures, are attractive because they can be made from readily available and highly tailorable metal and ligand precursors for multifunctional integration. Although their topological structure is amorphous in nature and leads to irregular porosity, functional ligand species could be vastly expanded and thus render versatile utility,<sup>15,16</sup> including catalysis,<sup>17,18</sup> separation,<sup>19,20</sup> optical imaging,<sup>21,22</sup> gas storage,<sup>23,24</sup> supercapacitance,<sup>25</sup> and biomolecule<sup>26,27</sup> and drug delivery.<sup>28–33</sup> With this in mind, designing a catalytically active ligand targeting a specific reaction would be possible. Due to the strong metal–ligand bonds, CPP acts as a scaffold to support the IL-based catalyst and allows for large interfacial surface area, where the catalytic active sites of ILs can be remarkably exposed. In addition, conjugation of CPPs with other functional materials is easily achieved and elaborately modulated. The produced hybrids have a well-defined core–shell nanostructure, expanding their scope of utilization. We envision a route that combines magnetic nanoparticles with CPPs to produce hierarchically structured nanoparticles, which can be used for facile separation. This will become an important complementary function to further optimize post-treatment of the reaction, promoting the recoverability of CPPs over multiple cycles.

Herein, we synthesized a novel magnetic CPP microsphere with a well-defined core-double-shell nanostructure, composed of a carbon-covered Fe<sub>3</sub>O<sub>4</sub> cluster (Fe<sub>3</sub>O<sub>4</sub>@C) and an IL-based coordination polymer outer shell serving as a catalytic layer for the cycloaddition of CO<sub>2</sub> with epoxides. The Fe<sub>3</sub>O<sub>4</sub>@C was constructed in a one-pot solvothermal synthesis to produce a Fe<sub>3</sub>O<sub>4</sub> assembled cluster as a core covered with amorphous carbon with abundant dangling carboxylic groups as the shell. Novel ligand-coupled ILs were chelated with In(III) ions, and the formed complexes were deposited onto the Fe<sub>3</sub>O<sub>4</sub>@C to yield a uniform, porous coordination polymer shell. Because a combination of ILs and Lewis acids is known to enhance the catalytic activity for the cycloaddition of CO<sub>2</sub> with epoxide,<sup>34,35</sup> a commonly used Lewis acid molecule, metallosalen complex, was designed to catenate imidazolium, resulting in dual catalytically active centers, i.e., electrophilic center from the salen complex and nucleophilic center from the IL. To the best of our knowledge, the present design to immobilize a bifunctional catalyst on a support of a porous CPP in a hybrid particle has never been reported. The larger interfacial surface of the CPP shell is expected to expose the bifunctional catalysts with synergistic effect for a great enhancement in catalytic efficiency and selectivity. Meanwhile, the multifunctional CPP catalysts could be easily recovered under external magnetic force due to the presence of the superparamagnetic core cluster.

## 2. EXPERIMENTAL SECTION

**2.1. Materials.** Ferrocene (Fe(C<sub>5</sub>H<sub>5</sub>)<sub>2</sub>, 99%), 4-bromobenzoic acid (98%), imidazole (99%), 1,2-cyclohexanediammonium monotartrate (99%), *para*-formaldehyde (96%) and tetrabutylammonium bromide (96%) were purchased from Aladdin Chemical Reagent Co., Ltd. 3-*tert*-Butyl-2-hydroxybenzaldehyde (96%) was purchased from Sigma-Aldrich Reagent Co., LLC. Diethylaluminum chloride (0.9 M solution in toluene) was purchased from J&K Scientific Ltd. All chemicals were used as received without further purification. Highly pure water (Millipore) of resistivity greater than 18.0 MΩ·cm was used in all experiments.

**2.1.1. Synthesis of HIBA·HCl (1).** The preparation of HIBA·HCl was performed according to a literature method with some modification.<sup>36</sup> A mixture of K<sub>2</sub>CO<sub>3</sub> (7.72 g, 0.056 mol), 4-bromobenzoic acid (4.00 g, 0.02 mol), imidazole (6.84 g, 0.1 mol) and CuSO<sub>4</sub>·5H<sub>2</sub>O (0.01 g, 4.0 × 10<sup>-5</sup> mol) was ground sufficiently in an agate mortar. Then, the powdered reactant mixture was transferred into a 100 mL Teflon-lined autoclave, which was sealed and kept at 200 °C for 10 h. After the reaction system was cooled to room temperature, the reaction mixture was dissolved in water and then filtered off. The filtrate was adjusted with dilute hydrochloric acid to pH 3.0–4.0 and then evaporated under reduced pressure. The crude product was recrystallized in ethanol, and 3.27 g of colorless needle crystals of HIBA·HCl was obtained (Yield: 65%, based on 4-bromobenzoic acid). <sup>1</sup>H NMR (400 MHz, DMSO-*d*<sub>6</sub>, δ): 13.11 (s, 1H, COOH), 8.40 (s, 1H, Im H), 8.02 (d, 2H, Ar H), 7.86 (s, 1H, Im H), 7.79 (d, 2H, Ar H), 7.13 (s, 1H, Im H).

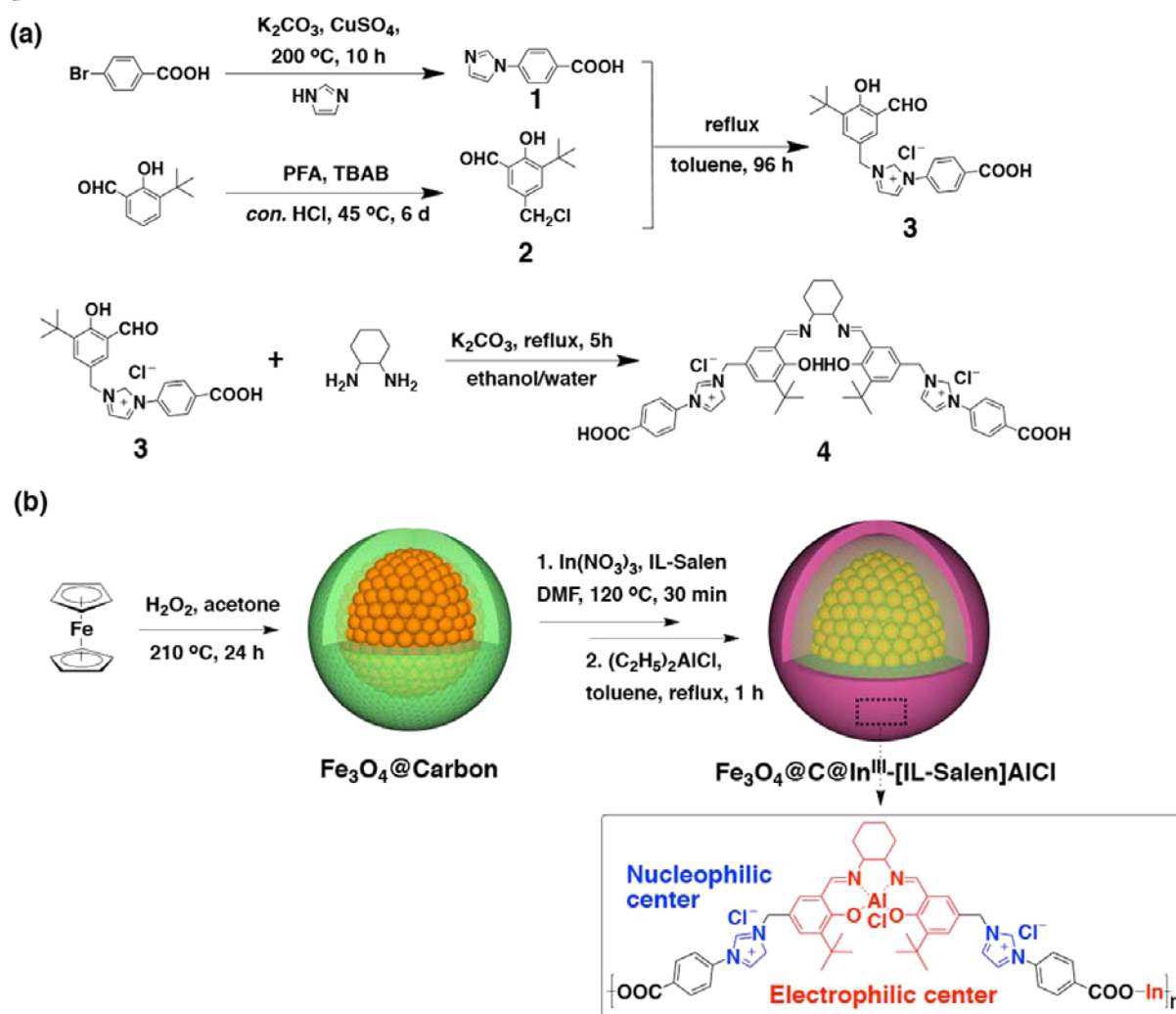
**2.1.2. Synthesis of 2-Hydroxy-3-*tert*-butyl-5-chloromethyl Benzaldehyde (2).** The preparation was performed following the literature.<sup>37</sup> 3-*tert*-Butyl-2-hydroxybenzaldehyde (2.7 g, 15.2 mmol) reacted with *para*-formaldehyde (1.0 g, 33.3 mmol) and tetrabutylammonium bromide (0.47 g, 1.46 mmol) in 11.0 mL of conc. hydrochloric acid under vigorous stirring at 45 °C for 6 days. The obtained products were extracted several times with diethyl ether. The organic phase was separated and washed with a saturated NaHCO<sub>3</sub> solution and brine. After drying on MgSO<sub>4</sub>, the product was concentrated to a yellow crystalline solid (3.4 g, yield: 99%). <sup>1</sup>H NMR (400 MHz, CDCl<sub>3</sub>, δ): 11.87 (s, 1H, OH), 9.88 (s, 1H, CHO), 7.53 (d, 1H, Ar H), 7.44 (d, 1H, Ar H), 4.59 (s, 2H, CH<sub>2</sub>Cl), 1.43 (s, 9H, *tert*-butyl).

**2.1.3. Synthesis of HIBA–Salicylaldehydes (3).** 2-Hydroxy-3-*tert*-butyl-5-chloromethyl Benzaldehyde (1.13 g, 5 mmol) and HIBA·HCl (1.12, 5 mmol) were added in 20 mL of toluene. The mixture was heated at reflux for 96 h. After the solution cooled to room temperature, the product was filtered, washed with toluene and dried under reduced pressure. Colorless crystalline solid was obtained (1.88 g, yield: 99%). <sup>1</sup>H NMR (400 MHz, DMSO-*d*<sub>6</sub>, δ): 13.43 (s, 1H, COOH), 11.84 (s, 1H, OH), 9.97 (s, 1H, CHO), 8.42 (s, 1H, Im H), 8.16 (d, 2H, Ar H), 8.11 (s, 1H, Im H), 7.93 (d, 2H, Ar H), 7.85 (s, 1H, Ar H), 7.77 (s, 1H, Ar H), 5.50 (s, 2H, CH<sub>2</sub>), 1.38 (s, 9H, *tert*-butyl). HRMS (ESI, *m/z*): [M + Cl]<sup>+</sup> calcd for C<sub>22</sub>H<sub>23</sub>N<sub>2</sub>O<sub>4</sub>, 379.43; found, 379.22. Anal. calcd for C<sub>22</sub>H<sub>23</sub>N<sub>2</sub>O<sub>4</sub>Cl·H<sub>2</sub>O, C 61.04, H 5.82, N 6.47; found, C 61.04, H 5.68, N 6.56.

**2.1.4. Synthesis of IL–Salen Ligands (4).** The preparation of IL–Salen ligands was performed according to the literature method.<sup>38</sup> Briefly, K<sub>2</sub>CO<sub>3</sub> (0.5 mmol) in water (2 mL) was added to a solution of HIBA–salicylaldehydes (0.5 mmol) and (1*R*,2*R*)-1,2-cyclohexanediammonium monotartrate (0.25 mmol) in ethanol (20 mL). The reaction mixture was heated at reflux for 5 h under nitrogen. The obtained yellow solid was collected by vacuum filtration, washed with ethanol several times and then evaporated under reduced pressure. HRMS (MALDI-TOF, *m/z*): [M + Cl]<sup>+</sup> calcd for C<sub>50</sub>H<sub>56</sub>N<sub>6</sub>O<sub>6</sub>Cl, 436.71; found, 437.24. [M + 2Cl]<sup>+</sup> calcd for C<sub>50</sub>H<sub>56</sub>N<sub>6</sub>O<sub>6</sub>Cl<sub>2</sub>, 454.42; found, 453.23. Anal. calcd for C<sub>50</sub>H<sub>56</sub>N<sub>6</sub>O<sub>6</sub>Cl<sub>2</sub>·2H<sub>2</sub>O, C 63.62, H 6.41, N 8.90; found, C 63.74, H 6.62, N 8.75.

**2.1.5. Synthesis of Fe<sub>3</sub>O<sub>4</sub>@Carbon Microspheres.** Fe<sub>3</sub>O<sub>4</sub>@carbon microspheres were synthesized following the reported protocol.<sup>39</sup> In a typical synthesis, ferrocene (0.6 g) was dissolved in 30 mL acetone. After intense sonication for 10 min, 3 mL H<sub>2</sub>O<sub>2</sub> was slowly added, and the mixture solution was vigorously stirred for 30 min. The precursor solution was then transferred to the Teflon-lined stainless autoclave with a total volume of 50.0 mL. The autoclave was heated and maintained at 210 °C for 24 h. After reaction, upon cooling to room temperature, the mixture was ultrasonically dispersed for 15 min, and the products were collected by a magnet, washed with acetone then ethanol three times and dried in a vacuum at 40 °C for 24 h.

**2.1.6. Synthesis of Fe<sub>3</sub>O<sub>4</sub>@C@In<sup>III</sup>-[IL–Salen] Microspheres.** Typically, Fe<sub>3</sub>O<sub>4</sub>@C microspheres (10 mg) were ultrasonically dispersed in 3 mL of DMF. To the above solution was added 20 μL DMF solution of In(NO<sub>3</sub>)<sub>3</sub> (0.66 mmol/mL). Then the mixture was transferred to a 25 mL three-necked flask and heated to 120 °C with vigorous stirring

Scheme 1. Schematic Illustration of Synthesis of IL-Salen Bifunctional Ligand (a) and  $\text{Fe}_3\text{O}_4@\text{C}@[\text{In}^{\text{III}}\text{-[IL-Salen]AlCl}$  Microsphere (b)

for 30 min. Afterward, 1 mL DMF solution of IL-Salen ligands ( $6.6\ \mu\text{mol/mL}$ ) was added dropwise into the above mixture solution within 5 min. The reaction was allowed to proceed for 1 h, during which the precipitates formed gradually. Finally, the as-obtained products  $\text{Fe}_3\text{O}_4@\text{C}@[\text{In}^{\text{III}}\text{-[IL-Salen]-1}$  were isolated by a magnet and washed with DMF and ethanol repetitively for further use.  $\text{Fe}_3\text{O}_4@\text{C}@[\text{In}^{\text{III}}\text{-[IL-Salen]-2}$  and  $\text{Fe}_3\text{O}_4@\text{C}@[\text{In}^{\text{III}}\text{-[IL-Salen]-3}$  were correspondingly synthesized by varying IL-Salen contents from 13.2 to  $26.4\ \mu\text{mol}$  under otherwise identical conditions.

**2.1.7. Synthesis of  $\text{Fe}_3\text{O}_4@\text{C}@[\text{In}^{\text{III}}\text{-[IL-Salen]AlCl}$  Microspheres.**  $\text{Fe}_3\text{O}_4@\text{C}@[\text{In}^{\text{III}}\text{-[IL-Salen]}$  microspheres (0.5 g) were dispersed in toluene (20 mL) under  $\text{N}_2$  atmosphere. Diethylaluminum chloride (0.063 mmol) in toluene (0.9 M, 0.07 mL) was added dropwise, and the mixture was heated under reflux for 1 h. The obtained products were isolated by a magnet and washed with DMF and ethanol.

**2.2. Typical procedure for Cycloadditions.**  $\text{Fe}_3\text{O}_4@\text{C}@[\text{In}^{\text{III}}\text{-[IL-Salen]AlCl}$  microspheres (0.1 g) and propylene oxide (PO) (20 mmol) were added into a 25 mL stainless-steel autoclave equipped with a magnetic stirrer, which had been previously dried at  $100\text{ }^\circ\text{C}$  under vacuum for 5 h. After the reaction mixture was heated to the desired temperature,  $\text{CO}_2$  was then charged into the reactor until the desired pressure was reached. After a certain time, the autoclave was placed into ice water and the remaining  $\text{CO}_2$  was slowly released in a cold trap containing ethyl acetate to absorb trace amounts of reactant and product entrained by  $\text{CO}_2$ . Then the ethyl acetate in the cold trap and the internal standard biphenyl for gas chromatography (GC) analysis were added into the reactor. The solid catalysts were separated

by using a magnet, were thoroughly washed with ethyl acetate, ethyl ether or DMF and dried under vacuum without further purification. Each catalytic reaction was repeated three times to ensure reproduction of results. The purity and structure of the product were analyzed by  $^1\text{H}$  NMR and GC-MS. To estimate the reusability of catalysts, the particles were collected out of the reaction mixtures by a magnet after they were subjected to the multiple cycloaddition reactions. Then the coordination polymer shells surrounding the particles were degraded into metal ions and ligands in the acidic solution. The quantitative assay of Al ions was conducted with inductively coupled plasma atomic emission spectroscopy (ICP-AES). After comparison with the initial concentrations, the leaching content of [IL-Salen]AlCl ligands could be calculated.

**2.3. Characterizations.**  $^1\text{H}$  NMR spectra was recorded on a Varian Mercury plus 400 MHz spectrophotometer at 298 K. Mass spectra (ESI) was measured by using a LTQ mass spectrometer, using methanol solutions of the sample. High resolution transmission electron microscopy (HR TEM) images were obtained on a JEM-2010 (JEOL, Japan) transmission electron microscope at an accelerating voltage of 200 kV. Samples dispersed at an appropriate concentration were cast onto a carbon-coated copper grid. Energy-dispersive X-ray (EDX) spectra were measured on the TEM instrument with an EDXS spectrometer. Magnetic characterization was carried out with a vibrating sample magnetometer (VSM) on a Model 6000 physical property measurement system (Quantum Design, USA) at 300 K. Fourier transform infrared (FT IR) spectra were recorded on a Magna-550 (Nicolet, USA) spectrometer. The samples were dried, mixed with



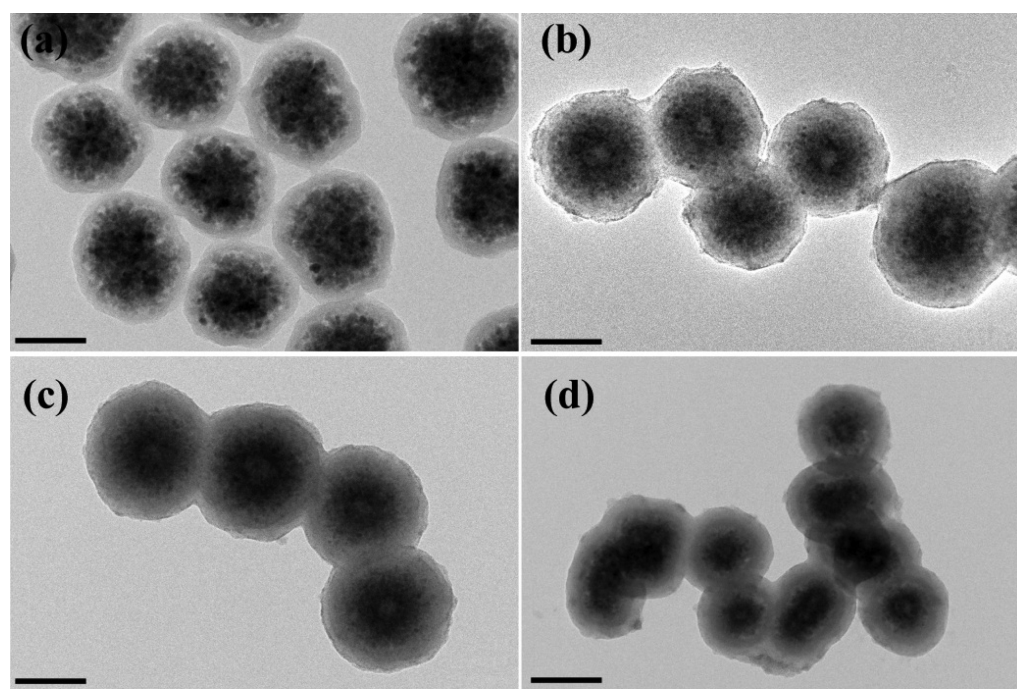


**Figure 1.** HR TEM images of  $\text{Fe}_3\text{O}_4@\text{C}$  (a),  $\text{Fe}_3\text{O}_4@\text{C}@\text{In}^{\text{III}}\text{-[IL-Salen]-1}$  (b),  $\text{Fe}_3\text{O}_4@\text{C}@\text{In}^{\text{III}}\text{-[IL-Salen]-2}$  (c) and  $\text{Fe}_3\text{O}_4@\text{C}@\text{In}^{\text{III}}\text{-[IL-Salen]-3}$  (d). Three magnetic CPP composites were correspondingly synthesized by varying IL-Salen contents from 6.6, 13.2 to 26.4  $\mu\text{mol/mL}$  under otherwise identical conditions ( $\text{Fe}_3\text{O}_4@\text{C}$ , 10 mg; molar ratio of In(III) IL-Salen: 2/1; DMF, 4 mL). The scale bars in panels a–c are 100 nm; the scale bar in panel d is 200 nm.

KBr and compressed to a plate for measurement. Hydrodynamic diameter ( $D_h$ ) was measured with a Nano ZS Zetasizer (model ZEN3600, Malvern Instruments) using a He–Ne laser at a wavelength of 632.8 nm. Nitrogen sorption measurements were performed at 77 K by an ASAP2020 volumetric adsorption analyzer (Micromeritics, USA). The samples were degassed at 120 °C for 12 h before measurement. Powder X-ray diffraction (PXRD) patterns were collected on a D8 advance (Bruker, Germany) diffractometer with Cu  $K\alpha$  radiation at  $\lambda = 0.154$  nm operating at 40 kV and 40 mA. ICP-AES was performed by a P-4010 (Hitachi, Japan) spectrometer. Thermogravimetric analysis (TGA) data was obtained with a Pyris-1 (PerkinElmer, USA) thermal analysis system under a flowing air atmosphere at a heating rate of 20 °C/min from 100 to 800 °C. Scanning electron microscopy (SEM) images were recorded on a SUPERSCAN SSX-550 electron microscope (Shimadzu, Japan) operating at 20 kV. A thin gold film was sprayed on the sample before measurements. The X-ray photoelectron spectroscopy (XPS) was performed using a PHI 5000C ESCA System X-ray photoelectron spectrometer.

### 3. RESULTS AND DISCUSSION

**3.1. Synthesis and Characterization of  $\text{Fe}_3\text{O}_4@\text{C}@\text{In}^{\text{III}}\text{-[IL-Salen]}$  Microspheres.** IL-Salen bifunctional ligand (4) with two branches containing imidazolium groups was synthesized following the procedure in Scheme 1a. First, imidazole was used as the starting material to react with 4-bromobenzoic acid to provide HIBA-HCl (1). Compound 1 was then reacted with 2-hydroxy-3-*tert*-butyl-5-chloromethyl benzaldehyde (2) to obtain the intermediate (3) in toluene. The mixture of intermediate (3) and (1*R*,2*R*)-1,2-cyclohexane diammonium monotartrate were heated in ethanol to give IL-Salen ligand (4) containing nucleophilic/electrophilic dual centers upon metal complexation with Salen moiety. Then a magnetic microsphere was prepared for supporting of IL-Salen ligands. As illustrated in Scheme 1b,  $\text{Fe}_3\text{O}_4@\text{C}$  microspheres were synthesized under solvothermal condition in one pot,

following the modified method in our previous report.<sup>25</sup> Coordination polymerization was subsequently carried out in the presence of  $\text{Fe}_3\text{O}_4@\text{C}$  microspheres. The abundant carboxylic groups formed on the surface of carbon shell<sup>39,40</sup> were used to chelate metal ions for locally induced growth of coordination polymer shells through the linkage of terminal carboxylic groups of IL-Salen ligands and In(III) ions. As the reaction progressed, the coordination polymer layer on the periphery of the  $\text{Fe}_3\text{O}_4@\text{C}$  template became thicker, and its growth was halted upon precipitation out of solution. Although the reaction time was quite short, the outer shell was uniform and attached strongly to the carbon surface. Thus, the synthesized hybrid structure was composed of a carbon inner shell and an  $\text{In}^{\text{III}}\text{-[IL-Salen]}$  coordination polymer outer shell surrounding the  $\text{Fe}_3\text{O}_4$  core, and it can be finely tuned by varying the shell thickness, pore size and magnetic properties. As reported earlier, In(III) ions are merely conjugated with the terminal carboxylic groups of ligands, and the  $\text{N}_2\text{O}_2$  coordination pocket of Salen is thus available to complex Al ions.<sup>33,41</sup> For comparison, the pure  $\text{In}^{\text{III}}\text{-[IL-Salen]}$  CPPs were ever synthesized by the same route, but the precipitates could not be formed in solution. We assumed that  $\text{Fe}_3\text{O}_4@\text{C}$  microspheres might serve as cross-linkers to trigger the deposition of the formed coordination polymers on the surface of carbon layer.

HR TEM was used to visualize the formation of core-double-shell microstructure. Figure 1a clearly shows the nanoparticle-assembled cluster core of  $\sim 130$  nm and uniform carbon shell of  $\sim 20$  nm around the  $\text{Fe}_3\text{O}_4$  supraparticles. Subjected to the successive precipitation polymerization through the binding of carboxylated IL-Salen ligands and In(III) ions, the magnetic composite nanoparticles were densely encapsulated by a metal–ligand layer of  $\sim 5$  nm. A close inspection of the outer shell in Figure 1b indicates a rough surface with discontinuous

coverage on the carbon shell. Fine control over the second layer in thickness and uniformity was then deliberately studied. The concentration of IL-Salen ligands increased from 13.2 to 26.4  $\mu\text{mol/mL}$  as the feeding amount of  $\text{Fe}_3\text{O}_4@\text{C}$  nanoparticles was constant. Figure 1c,d displays the changing tendency of the second shell. In comparison to the primary view in Figure 1b, the overall sizes of the resulting microspheres were up to approximately 200 and 260 nm, implying that the coordination polymer shell was increased to  $\sim 15$  and  $\sim 45$  nm, respectively. Accompanied with the increment of shell sizes, the texture of coordination polymer shell appeared more solid and compacted. SEM images also display a quite rough and grained surface upon the covering of a thick coordination polymer shell (Figure S1 in the Supporting Information). The hydrodynamic diameter ( $D_h$ ) of different microspheres was measured by dynamic light scattering (DLS). The average  $D_h$  value of  $\text{Fe}_3\text{O}_4@\text{C}$  microspheres was 304 nm. Upon formation of the second shell, the sizes of the microspheres increased from 395 to 471 nm depending on the concentration of IL-Salen ligands. Again, this result validates the same concentration-dependent growth of the coordination polymer shell (Table S1 in the Supporting Information).

To qualitatively examine the components of the resulting microspheres, a series of measurements were conducted. Powder X-ray diffraction (PXRD) was applied to analyze the crystalline properties of  $\text{Fe}_3\text{O}_4@\text{C}@[\text{In}^{\text{III}}\text{-IL-Salen}]$  microspheres. It can be seen that  $\text{Fe}_3\text{O}_4@\text{C}$  microspheres gave five characteristic diffraction peaks that could all be indexed to the cubic structure of  $\text{Fe}_3\text{O}_4$  (JCPDS No.75-1609) (Figure S2 in the Supporting Information). After  $\text{Fe}_3\text{O}_4@\text{C}$  nanoparticles were heavily wrapped by coordination polymers, the signals due to  $\text{Fe}_3\text{O}_4$  nanocrystals became weak. Also, because the coordination polymer shell is rapidly formed by a way of solvent-induced precipitation as used before,<sup>23,25</sup> its structure was amorphous and only give a broad peak at  $\theta = 24.1^\circ$  in the PXRD pattern. Energy dispersive X-ray (EDX) spectroscopy was acquired to perform the elemental analysis of the core-double-shell particles; both Fe and In atoms were observed (Figure S3a in the Supporting Information). The elemental mapping from EDX revealed that the abundant Fe atoms predominately resided in the core region, while the rarer In atoms were evenly distributed throughout the particle (Figure S3b in the Supporting Information), indicating a homogeneous covering of coordination polymers. Thermogravimetric analysis (TGA) (Figure 2a) was performed in air to quantitatively analyze the component contents of the  $\text{Fe}_3\text{O}_4@\text{C}@[\text{In}^{\text{III}}\text{-IL-Salen}]$  microspheres. In all samples, it was shown that the organic components completely decomposed below 400  $^\circ\text{C}$ , while the inorganic components remained. According to the mass loss from the TGA curves, the weight percentages of  $\text{Fe}_3\text{O}_4$  cluster, carbon and coordination polymer could be calculated. With the increase of the outer layer from  $\sim 5$ ,  $\sim 15$  to  $\sim 45$  nm, the loadings of IL-Salen bifunctional catalysts reached 13.72%, 16.90% and 28.51% respectively, which are far greater than those of the chemically grafted SILCs.

Magnetic properties of the composite microspheres were studied using a vibrating sample magnetometer at 300 K in an external magnetic field (Figure 2b). As compared to the  $\text{Fe}_3\text{O}_4@\text{C}$  nanoparticles, the saturation magnetization values of the magnetic composite CPPs decreased from 33 to 25, 21 and 12 emu/g as the sizes of the coordination polymer shells increased. The data was then used to calculate the magnetic contents, which varied from 13.1%, 16.5% to 26.1%. This is in

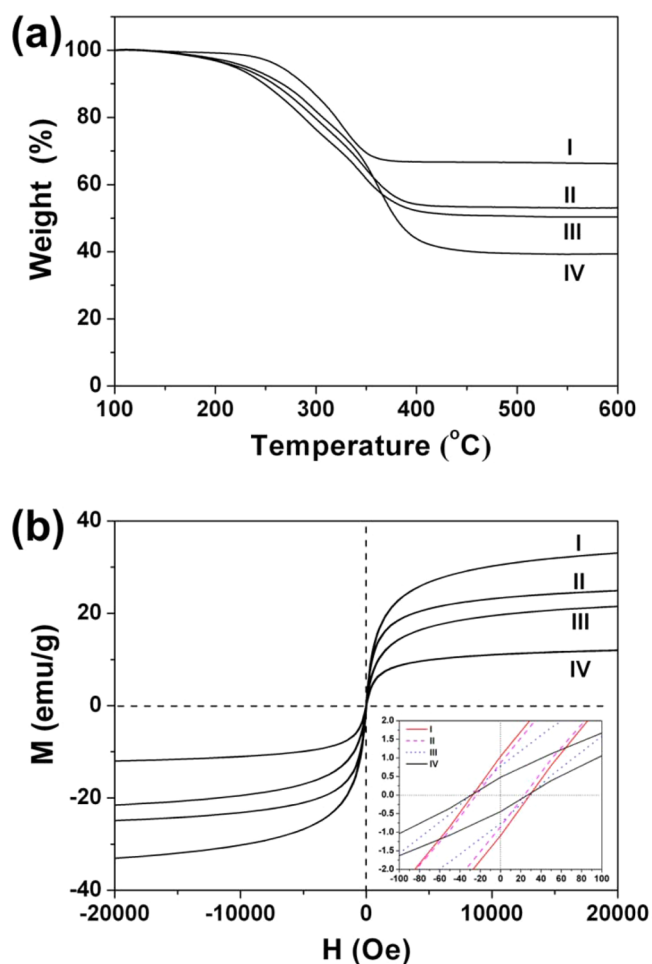


**Figure 2.** TGA curves (a) and magnetic hysteresis curves (b) of  $\text{Fe}_3\text{O}_4@\text{C}$  (I),  $\text{Fe}_3\text{O}_4@\text{C}@[\text{In}^{\text{III}}\text{-IL-Salen}]-1$  (II),  $\text{Fe}_3\text{O}_4@\text{C}@[\text{In}^{\text{III}}\text{-IL-Salen}]-2$  (III) and  $\text{Fe}_3\text{O}_4@\text{C}@[\text{In}^{\text{III}}\text{-IL-Salen}]-3$  (IV). The inset in panel b is the magnified view of magnetic hysteresis curves in the region of low magnetic field.

agreement to the data calculated from the TGA curves. The inset of Figure 2b depicts an enlarged section of the magnetization plot near the zero magnetic field. Saturation remanence and coercivity were determined from the intersection of the hysteresis loop with the two axes. The findings for all samples prove that a minor residual magnetization was present upon removal of the external magnetic field, and only a low-intensity magnetic field was required to reduce the magnetization to zero. This is evidence that the inclusive  $\text{Fe}_3\text{O}_4$  nanocrystals are in the superparamagnetic state.

The porosity of the composite microspheres was studied to determine whether the coordination polymer shell had interstices given by the metal–ligand topological framework. Figure 3 shows the gas sorption isotherms measured by using  $\text{N}_2$  sorption analysis at 77 K. All samples showed the type-IV gas sorption isotherms, according to the IUPAC classification, indicative of a mesopore character. Different hysteresis loops were observed between the branches of adsorption and desorption isotherms. Apart from the sample with the maximum uptake of  $\text{N}_2$ , the others rendered similar hysteresis loops at  $P/P_0 > 0.9$ , which implied that large mesopores were present due to the loose accumulation of particles. The increased coordination polymer shell also led the hysteresis loops to move toward the low-pressure region (Figure 3IV).

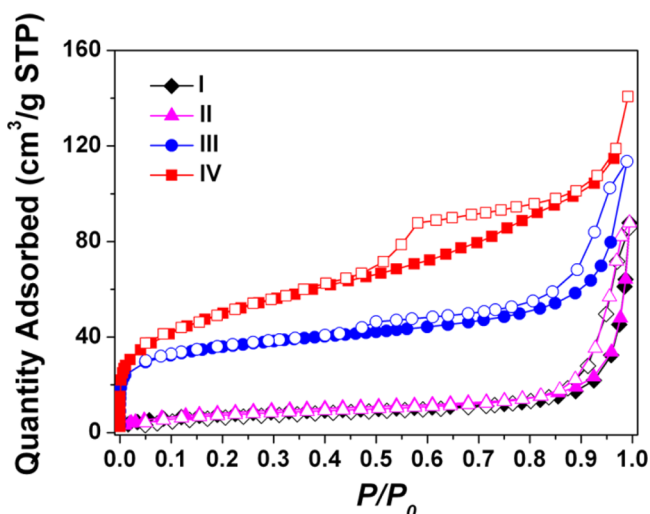


**Figure 3.** Nitrogen sorption isotherms of  $\text{Fe}_3\text{O}_4@\text{C}$  (I),  $\text{Fe}_3\text{O}_4@\text{C}@\text{In}^{\text{III}}\text{-}[\text{IL-Salen}]\text{-1}$  (II),  $\text{Fe}_3\text{O}_4@\text{C}@\text{In}^{\text{III}}\text{-}[\text{IL-Salen}]\text{-2}$  (III) and  $\text{Fe}_3\text{O}_4@\text{C}@\text{In}^{\text{III}}\text{-}[\text{IL-Salen}]\text{-3}$  (IV).

Using the Brunauer–Emmett–Teller (BET) model, the total pore volumes and surface areas were compiled in Table 1.

**Table 1.** Porosity Parameters of  $\text{Fe}_3\text{O}_4@\text{C}$  and a Series of  $\text{Fe}_3\text{O}_4@\text{C}@\text{In}^{\text{III}}\text{-}[\text{IL-Salen}]$  Samples Characterized by Nitrogen Isotherm Adsorption

| sample  | $S_{\text{BET}}$ ( $\text{m}^2/\text{g}$ ) <sup>a</sup> | $V_p$ ( $\text{cm}^3/\text{g}$ ) <sup>b</sup> |
|---|---|---|
| $\text{Fe}_3\text{O}_4@\text{C}$  | 28.2 (50.3)   | 0.1325  |
| $\text{Fe}_3\text{O}_4@\text{C}@\text{In}^{\text{III}}\text{-}[\text{IL-Salen}]\text{-1}$ | 37.2 (83.9)   | 0.1472  |
| $\text{Fe}_3\text{O}_4@\text{C}@\text{In}^{\text{III}}\text{-}[\text{IL-Salen}]\text{-2}$ | 117.0 (179.3)   | 0.1532  |
| $\text{Fe}_3\text{O}_4@\text{C}@\text{In}^{\text{III}}\text{-}[\text{IL-Salen}]\text{-3}$ | 174.7 (282.4)   | 0.2175  |

<sup>a</sup>Surface area is calculated from the nitrogen sorption isotherms using the Brunauer–Emmett–Teller method, and the value in parentheses is the Langmuir surface area. <sup>b</sup>Total pore volume at  $P/P_0 = 0.99$ .

$\text{Fe}_3\text{O}_4@\text{C}$  affords a low specific surface area of  $28.23 \text{ m}^2/\text{g}$  and a pore volume of  $0.1325 \text{ cm}^3/\text{g}$ . Upon further modification with coordination polymers, the surface areas showed a pronounced increase due to substantial coverage with the metal–ligand framework. Of the three  $\text{Fe}_3\text{O}_4@\text{C}@\text{In}^{\text{III}}\text{-}[\text{IL-Salen}]$  particles, the greatest specific surface area and pore volume,  $174.7 \text{ m}^2/\text{g}$  and  $0.2175 \text{ cm}^3/\text{g}$  respectively, were found with  $\text{Fe}_3\text{O}_4@\text{C}@\text{In}^{\text{III}}\text{-}[\text{IL-Salen}]\text{-3}$ , which had the largest coordination polymer shell. The mesopore-size distributions were calculated using the Barret–Joyner–Halenda (BJH) model. As shown in Figure 4, the size populations of the four samples showed a clear trend; as the coordination polymer shell increased, the dominant mesopore sizes moved from the region of 20–30 nm to 3–5 nm. In addition to the mesopores, the micropores (<2 nm) were also formed in the thick coordination polymer shells around the  $\text{Fe}_3\text{O}_4@\text{C}$  particles. The nonlocal density functional theory (NLDFT) model was applied to analyze the microporosity. One can see that the  $\text{Fe}_3\text{O}_4@\text{C}@\text{In}^{\text{III}}\text{-}[\text{IL-Salen}]\text{-2}$  and -3 particles both afforded the micropores with the dominant sizes of 1.0–1.5 nm (Figure S4 in the Supporting Information). This gives efficient access for the substrates, and also is conducive to enhance the catalytic efficiency and selectivity within mesoporous channels.

**3.2. Immobilization of  $\text{AlCl}_3^{2+}$  into  $\text{Fe}_3\text{O}_4@\text{C}@\text{In}^{\text{III}}\text{-}[\text{IL-Salen}]$  Microspheres.** The  $\text{N}_2\text{O}_2$  coordination pocket of IL-

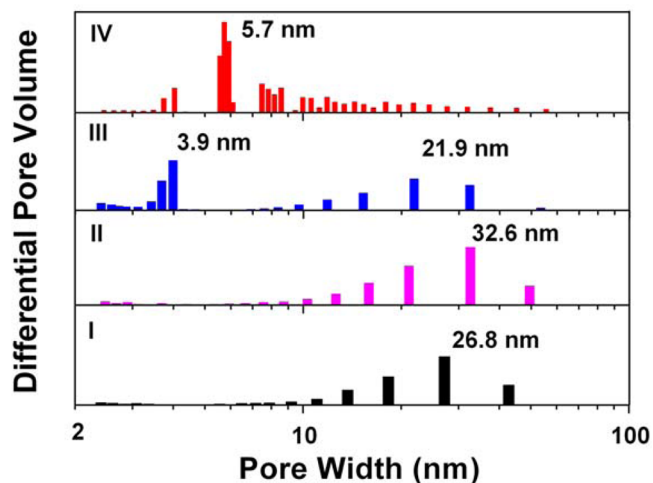
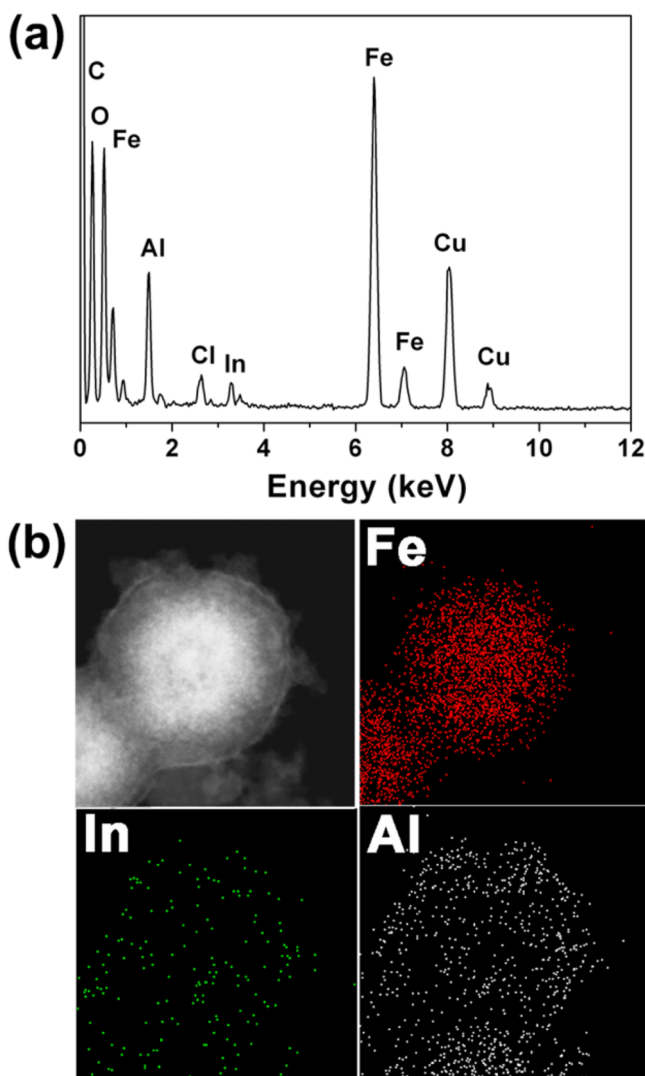


**Figure 4.** Pore-size distributions of  $\text{Fe}_3\text{O}_4@\text{C}$  (I),  $\text{Fe}_3\text{O}_4@\text{C}@\text{In}^{\text{III}}\text{-}[\text{IL-Salen}]\text{-1}$  (II),  $\text{Fe}_3\text{O}_4@\text{C}@\text{In}^{\text{III}}\text{-}[\text{IL-Salen}]\text{-2}$  (III) and  $\text{Fe}_3\text{O}_4@\text{C}@\text{In}^{\text{III}}\text{-}[\text{IL-Salen}]\text{-3}$  (IV), calculated by BJH model.

Salen ligands was used to chelate  $\text{AlCl}_3^{2+}$ , which will function as the electrophilic center for the catalytic microspheres. To validate their presence, the EDX spectrum of  $\text{AlCl}_3^{2+}$ -modified microspheres is shown in Figure 5a. Excluding the Fe and In atoms, the characteristic peaks from Cl and Al atoms were found in the spectrum. Combined with the elemental mapping (Figure 5b), the result explicitly reveals the specific core–shell microstructure, wherein Fe atoms are distributed in the core region, while In and Al atoms are spread throughout the whole shell.

To further examine the chelating linkage between  $\text{AlCl}_3^{2+}$  and  $\text{N}_2\text{O}_2$  structure of IL-Salen ligands, X-ray photoelectron spectroscopy (XPS) was performed for  $\text{Fe}_3\text{O}_4@\text{C}@\text{In}^{\text{III}}\text{-}[\text{IL-Salen}]$  and  $\text{Fe}_3\text{O}_4@\text{C}@\text{In}^{\text{III}}\text{-}[\text{IL-Salen}]\text{AlCl}$  microspheres (Figure S5 in the Supporting Information). The peaks of  $\text{Al}(2s)$ ,  $\text{Al}(2p)$  and  $\text{Cl}(2p^3)$  appeared in the spectrum upon immobilization of  $\text{AlCl}_3^{2+}$  by multidentate sites; moreover, the binding energy of  $\text{O}(1s)$  was found to shift from 533.4 (O–C) to 531.6 eV (O–Al) (Figure 6a), suggesting the formation of Al–O bond.<sup>42</sup> FT IR spectroscopy was then used to confirm the polymerization and coordination of  $\text{AlCl}_3^{2+}$  (Figure 6b). Numerous carboxylic groups on the surface of carbon shell are exposed to trigger the precipitation of  $\text{In}^{\text{III}}$ –carboxylate coordination polymers on the  $\text{Fe}_3\text{O}_4@\text{C}$  microspheres. The formed CPP composite gives a characteristic stretching vibration at  $1655 \text{ cm}^{-1}$  for the C=O bond that originated from the coordinated carboxylic groups; this is a shift of  $45 \text{ cm}^{-1}$  from the original C=O of carboxylic groups ( $1700 \text{ cm}^{-1}$ ) attached to the carbon shell of  $\text{Fe}_3\text{O}_4@\text{C}$  microspheres, which also involve numerous C=C bonds resulting in a characteristic vibration at  $1625 \text{ cm}^{-1}$ .<sup>43</sup> Simultaneously, the peak appearing at  $1555 \text{ cm}^{-1}$  is ascribed to the stretching vibration for the C=N bond of the Salen moiety in the coordination polymer shell. Once  $\text{AlCl}_3^{2+}$  is bound to the IL-Salen component, the aforementioned two peaks are both blue-shift from 1655 to  $1678 \text{ cm}^{-1}$  and 1555 to  $1643 \text{ cm}^{-1}$  because of the coordination effect between Al and imine. Also, the peak at  $625 \text{ cm}^{-1}$  becomes broader, which can be attributed to the stretching vibration of Al–O bonds of the octahedrally coordinated Al.<sup>44</sup> The quantitative analysis using ICP-AES disclosed 2.7 wt % of Al atoms remained within  $\text{Fe}_3\text{O}_4@\text{C}@\text{In}^{\text{III}}\text{-}[\text{IL-Salen}]\text{AlCl}$ -3

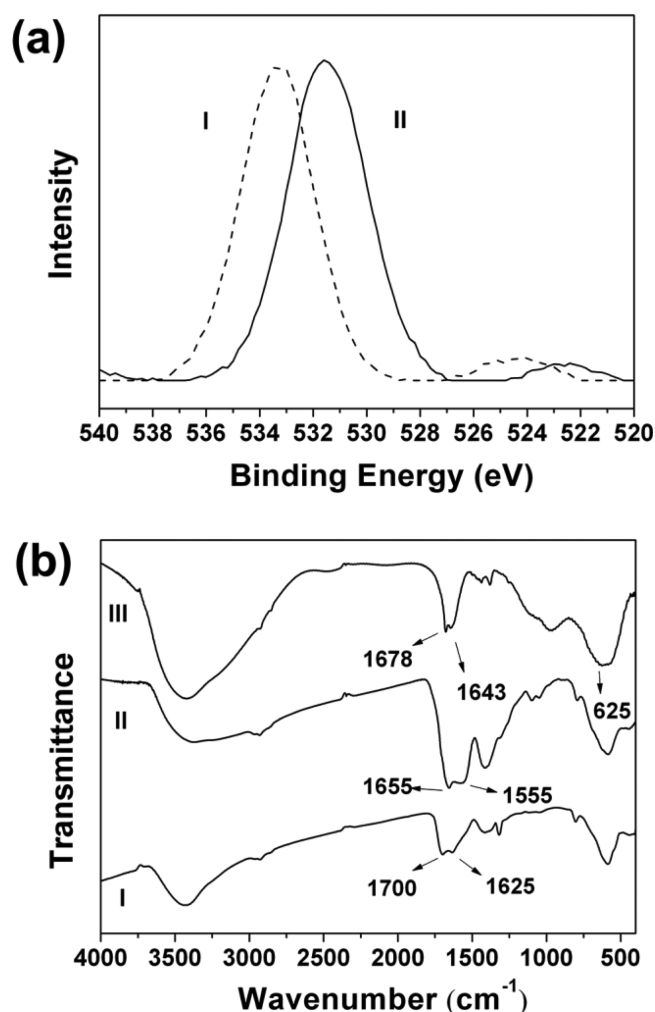




**Figure 5.** EDX spectrum (a) and elemental mapping (b) of  $\text{Fe}_3\text{O}_4@\text{C}@[\text{In}^{\text{III}}\text{-[IL-Salen]AlCl}$ .

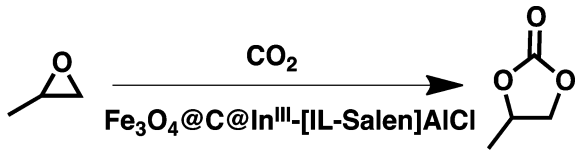
microspheres, which was comparable to the theoretical value (1.7 wt %).

**3.3. Evaluation of Catalytic Activity of  $\text{Fe}_3\text{O}_4@\text{C}@[\text{In}^{\text{III}}\text{-[IL-Salen]AlCl}$  Microspheres for Cycloaddition Reaction.** To assess the catalytic performance of  $\text{Fe}_3\text{O}_4@\text{C}@[\text{In}^{\text{III}}\text{-[IL-Salen]AlCl}$ , we employed propylene oxide (PO) as a model compound to fix  $\text{CO}_2$  by cycloaddition reaction. A systematic investigation was undertaken to examine the influence of reaction parameters ( $\text{CO}_2$  pressure, additive, reaction time and temperature) on the yield of cyclic carbonates, and the results are compiled in Table 2. As a control, the metallosalen containing two terminal carboxylic groups was synthesized and used as a ligand to encapsulate the  $\text{Fe}_3\text{O}_4@\text{C}$  particles by the coordination precipitation polymerization with  $\text{In}(\text{III})$  ions. The formed  $\text{Fe}_3\text{O}_4@\text{C}@[\text{In}^{\text{III}}\text{-[Salen]AlCl}$  was nonporous in a polymer shell, differing from the high-surface-area structure of IL-functionalized microspheres. As expected, without ammonium salts used as cocatalysts, nearly no product was detected (entry 1) by using the monofunctional catalysts. Addition of 2.5% tetrabutyl ammonium bromide (*n*-TBAB) led to 34.5% yield of the corresponding product (entry 2). But if *n*-TBAB (2.5%) was used alone, only 6.8% yield could be obtained (entry 3). It has been proved that *n*-TBAB could directly



**Figure 6.** (a) O(1s) XPS spectra of  $\text{Fe}_3\text{O}_4@\text{C}@[\text{In}^{\text{III}}\text{-[IL-Salen]}$  (I) and  $\text{Fe}_3\text{O}_4@\text{C}@[\text{In}^{\text{III}}\text{-[IL-Salen]AlCl}$  (II). (b) FT IR spectra of  $\text{Fe}_3\text{O}_4@\text{C}$  (I),  $\text{Fe}_3\text{O}_4@\text{C}@[\text{In}^{\text{III}}\text{-[IL-Salen]}$  (II) and  $\text{Fe}_3\text{O}_4@\text{C}@[\text{In}^{\text{III}}\text{-[IL-Salen]AlCl}$  (III).

catalyze the chemical fixation of  $\text{CO}_2$  onto epoxides.<sup>45</sup> However, the reaction temperature must be increased above  $100\text{ }^\circ\text{C}$  to melt *n*-TBAB as a reaction solvent. Apparently, this is not in our case. Following the initial trial, the  $\text{Fe}_3\text{O}_4@\text{C}@[\text{In}^{\text{III}}\text{-[IL-Salen]AlCl}$  particles with *n*-TBAB (2.5%) were employed to catalyze the cycloaddition of  $\text{CO}_2$  to PO under the identical conditions. Compared to the activity of monofunctional particles, the yield of bifunctional catalysts dramatically increased to 96.5% (entry 4). It is likely that the high surface area of catalytic shell facilitates the improvement of adsorbed capacity and rate of  $\text{CO}_2$  gas and the ease of the nucleophilic attack by the bromide ion of *n*-TBAB. Also, this improvement encouraged us to evaluate their catalytic activity in the form of single component without the use of cocatalysts. At low temperature ( $40\text{ }^\circ\text{C}$ ), they merely presented a very low yield (entry 5). But the remarkable enhancement of reaction efficiency was obtained as the reaction was heated to  $100\text{ }^\circ\text{C}$  (entry 6), and a longer reaction time could eventually give the best yield (entry 7). Also, there was no other product such as polycarbonate detected with  $^1\text{H}$  NMR and GC–MS, indicative of their excellent selectivity (>99%) toward cyclic carbonates. In general, the cycloaddition reaction is more sensitive to temperature compared to the other similar catalytic systems.

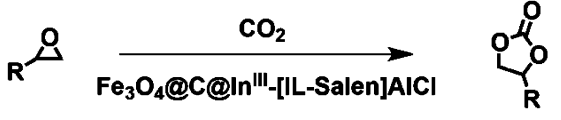
Table 2. Results of the Cycloaddition of CO<sub>2</sub> on PO under Various Conditions<sup>a</sup>


| entry | catalyst  | <i>n</i> -TBAB (mol %) | time (h) | temperature (°C) | <i>P</i> <sub>CO<sub>2</sub></sub> (MPa) | yield (%) <sup>b</sup> |
|-------|---|------------------------|----------|------------------|--|------------------------|
| 1     | Fe <sub>3</sub> O <sub>4</sub> @C@In <sup>III</sup> -[Salen]AlCl    | 0                      | 5        | 40               | 3  | n.d.                   |
| 2     | Fe <sub>3</sub> O <sub>4</sub> @C@In <sup>III</sup> -[Salen]AlCl    | 2.5                    | 5        | 40               | 3  | 34.5                   |
| 3     | none  | 2.5                    | 5        | 40               | 3  | 6.8                    |
| 4     | Fe <sub>3</sub> O <sub>4</sub> @C@In <sup>III</sup> -[IL-Salen]AlCl | 2.5                    | 5        | 40               | 3  | 96.5                   |
| 5     | Fe <sub>3</sub> O <sub>4</sub> @C@In <sup>III</sup> -[IL-Salen]AlCl | 0                      | 5        | 40               | 3  | 11.9                   |
| 6     | Fe <sub>3</sub> O <sub>4</sub> @C@In <sup>III</sup> -[IL-Salen]AlCl | 0                      | 5        | 100              | 3  | 75.6                   |
| 7     | Fe <sub>3</sub> O <sub>4</sub> @C@In <sup>III</sup> -[IL-Salen]AlCl | 0                      | 12       | 100              | 3  | 94.3                   |

<sup>a</sup>Reaction conditions: a stainless autoclave of 25 mL, 20 mmol PO, 0.1 g of catalysts. <sup>b</sup>The yields were determined by GC using biphenyl as the internal standard; n.d., not determined.

We assume that the high surface area of the coordination polymer shells with the bifunctional catalytic sites could significantly enhance the capability of CO<sub>2</sub> capture. Also, the gas–liquid diffusion rates are improved at elevated temperature and high CO<sub>2</sub> pressure by decreasing the viscosity of the liquid phase mixture. On the other hand, carboxylic acid is a strong Brønsted acid and hydrogen bond donor. It has been reported that the –COOH-modified ILs could accelerate the ring opening of epoxides.<sup>46</sup> Thus, the remaining carboxylic groups on the IL-functionalized metallosalen ligands would greatly promote the catalytic activity of bifunctional catalysts toward the cycloaddition reaction of CO<sub>2</sub> to epoxides.

Apart from PO, we examined the application scope of the cycloaddition reaction of CO<sub>2</sub> to various epoxides, using the high-surface-area Fe<sub>3</sub>O<sub>4</sub>@C@In<sup>III</sup>-[IL-Salen]AlCl-3 microspheres without any additives. As shown in Table 3, most substrates could be smoothly converted to the corresponding cyclic carbonates with high yields. Steric and electronic effects both played an important role. The electron-withdrawing nature of chloromethyl group on epichlorohydrin tended to promote the cycloaddition reaction within 4 h under otherwise identical conditions (entry 2), thereby generating a higher turn over frequency (TOF). Unfortunately, cyclohexene oxide exhibited the lower conversion even with the reaction time extended to 24 h (entry 4). This is possibly attributed to the steric hindrance that may limit the nucleophilic attack to the coordinated epoxide on the Lewis acid metal center. For 1,2-epoxyhexane with a linear long alkyl chain, the moderate yield was obtained (entry 3), presumably due to the poor dispersibility of the catalyst particles in epoxide substrate. Taking all of the results into account, the reaction mechanism of the bifunctional catalysts possibly complies with the reported monometallic pathway involving two nucleophiles for cyclic carbonate synthesis.<sup>47</sup> For comparison, Fe<sub>3</sub>O<sub>4</sub>@C@In<sup>III</sup>-[IL-Salen]AlCl-1 microspheres with reduced IL-[Salen]AlCl content (13.72%) and lower surface area (37.2 m<sup>2</sup>/g) were subjected to the cycloaddition reaction of PO and CO<sub>2</sub> under otherwise identical conditions, but gave rise to a low yield and

Table 3. Synthesis of Various Cyclic Carbonates from Epoxides 1-6 and CO<sub>2</sub> Catalyzed by Different Fe<sub>3</sub>O<sub>4</sub>@C@In<sup>III</sup>-[IL-Salen]AlCl Microspheres in the Presence of *n*-Bu<sub>4</sub>NBr<sup>a</sup>


| entry          | epoxide | time (h) | TOF (h <sup>-1</sup> ) | yield (%) <sup>b</sup> |
|----------------|---------|----------|------------------------|------------------------|
| 1              | 1       | 12       | 49                     | 94.3                   |
| 2              | 2       | 4        | 156                    | 92.8                   |
| 3              | 3       | 12       | 28                     | 80.6                   |
| 4              | 4       | 24       | 6.3                    | 46.1                   |
| 5              | 5       | 12       | 52                     | 95.9                   |
| 6 <sup>c</sup> | 6       | 12       | 47                     | 93.5                   |
| 7 <sup>d</sup> | 1       | 12       | 8.5                    | 38.0                   |

<sup>a</sup>Reaction conditions: 20 mmol epoxide, 0.1 g of Fe<sub>3</sub>O<sub>4</sub>@C@In<sup>III</sup>-[IL-Salen]AlCl-3, reaction temperature 100 °C, CO<sub>2</sub> pressure 3.0 MPa. <sup>b</sup>The yields were determined by GC with an internal standard biphenyl. <sup>c</sup>CO<sub>2</sub> pressure 6.0 MPa. <sup>d</sup>0.21 g of Fe<sub>3</sub>O<sub>4</sub>@C@In<sup>III</sup>-[IL-Salen]AlCl-1 particles was used to ensure the similar content of IL-[Salen]AlCl component as before.

TOF. This implies that the high-surface-area porous structure makes catalytically active sites evenly distributed throughout the whole shell rather than the confined surface of microspheres, as well as improvement of CO<sub>2</sub> capture.

To investigate the reusability and recoverability of catalysts, Fe<sub>3</sub>O<sub>4</sub>@C@In<sup>III</sup>-[IL-Salen]AlCl-3 was used in the cycloaddition reactions of PO with CO<sub>2</sub> over six cycles under the optimized conditions. After each run, the Fe<sub>3</sub>O<sub>4</sub> core enclosed within the microspheres could be used to harvest the catalysts out of the reaction mixture with the assistance of a magnet. As shown in Figure 7, high yields are attained in all six reaction runs, and accompanied by this trend, the cumulative leaching of [IL-Salen]AlCl ligands could also be ignored, less than 1.2%. The results indicate that Fe<sub>3</sub>O<sub>4</sub>@C@In<sup>III</sup>-[IL-Salen]AlCl

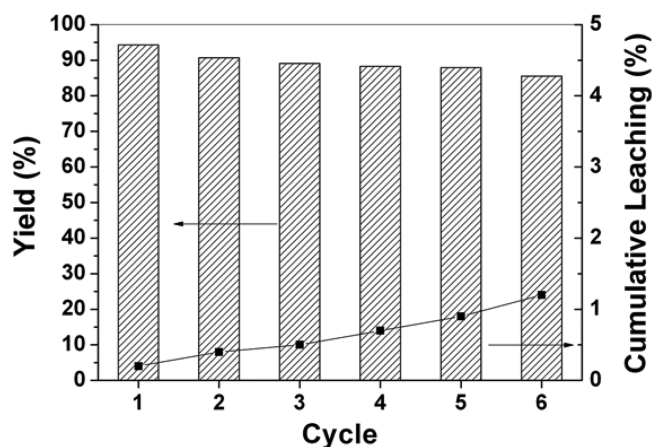


Figure 7. Recycle test of the composite catalysts and the monitoring of cumulative leaching of [IL-Salen]AlCl ligands using ICP-AES.



microspheres exhibit excellent reusability and stability for repetitive use in cycloaddition reactions.

#### 4. CONCLUSIONS

To summarize, multifunctional core-double-shell CPPs were synthesized by template-mediated coordination polymerization. Specifically,  $\text{Fe}_3\text{O}_4@C$  microspheres were solvothermally prepared to serve as a nanoplatform for the in situ formation of coordination polymer shell by virtue of abundant carboxylic groups on the carbon layer.  $\text{In(III)}$  ions were chelated with  $-\text{COOH}$  terminated imidazolium-substituted Salen bifunctional ligands, to produce the homogeneous second shell with controllable thickness. They possessed a fraction of fine mesopores with large surface area and pore volume, leading to potential electrophilic/nucleophilic synergistic properties and high gas adsorption capacity. Upon immobilization of  $\text{AlCl}_3^{2+}$  into the pocket of the salen moiety on the synthesized CPPs, the cycloaddition reaction of  $\text{CO}_2$  with epoxides was intensively studied by a series of  $\text{Fe}_3\text{O}_4@C@In^{III}\text{-[IL-Salen]-AlCl}_3$  microspheres with the varied surface areas. It was found that numerous catalytic sites within the framework of shell were available to epoxide substrates. The large surface area of the mesopores allowed for  $\text{CO}_2$  uptake and occurrence of cycloaddition reaction. The combination of the bifunctional catalysts afforded high yield and selectivity to cyclic carbonates. Also, the remaining carboxylic groups on the coordination polymer shells facilitate the acceleration of cycloaddition reaction. In addition to magnetic enrichment and catalytic stability during recycling, all of the results substantially demonstrate that  $\text{Fe}_3\text{O}_4@C@In^{III}\text{-[IL-Salen]-AlCl}_3$  microspheres are attractive toward the development of solid catalysts for the coupling of  $\text{CO}_2$  with epoxides. Along this line, we speculate that engineering of desired modules into CPP is a versatile and universal strategy to construct functions in quest of complexity, utility and adaptability of nanomaterials.

#### ■ ASSOCIATED CONTENT

##### Supporting Information

SEM images, PXRD patterns, EDS spectrum, elemental mappings, XPS spectra, micropore analysis and hydrodynamic diameters. This material is available free of charge via the Internet at <http://pubs.acs.org>.

#### ■ AUTHOR INFORMATION

##### Corresponding Author

\*J. Guo. E-mail: [guojia@fudan.edu.cn](mailto:guojia@fudan.edu.cn).

##### Notes

The authors declare no competing financial interest.

#### ■ ACKNOWLEDGMENTS

We acknowledge the financial support of the NSFC (Grant No. 21474015) and STCSM (Nos. 13520720200 and 14ZR1402300).

#### ■ REFERENCES

- (1) Han, L.; Li, H.; Choi, S. J.; Park, M. S.; Lee, S. M.; Kim, Y. J.; Park, D. W. Ionic Liquids Grafted on Carbon Nanotubes as Highly Efficient Heterogeneous Catalysts for the Synthesis of Cyclic Carbonates. *Appl. Catal., A* **2012**, *429–430*, 67–72.
- (2) Yang, J.; Zhang, Q. H.; Zhu, L. Y.; Zhang, S. G.; Li, J.; Zhang, X. P.; Deng, Y. Q. Novel Ionic Liquid Crystals Based on N-Alkylcaprolactam as Cations. *Chem. Mater.* **2007**, *19*, 2544–2550.

- (3) Parvulescu, V. I.; Hardacre, C. Catalysis in Ionic Liquids. *Chem. Rev.* **2007**, *107*, 2615–65.

- (4) Dai, W. L.; Luo, S. L.; Yin, S. F.; Au, C. T. The Direct Transformation of Carbon Dioxide to Organic Carbonates over Heterogeneous Catalysts. *Appl. Catal., A* **2009**, *366*, 2–12.

- (5) Zhang, Q.; Zhang, S.; Deng, Y. Recent Advances in Ionic Liquid Catalysis. *Green Chem.* **2011**, *13*, 2619–2637.

- (6) Shim, H. L.; Udayakumar, S.; Yu, J. L.; Kim, I.; Park, D. W. Synthesis of Cyclic Carbonate from Allyl Glycidyl Ether and Carbon Dioxide Using Ionic Liquid-Functionalized Amorphous Silica. *Catal. Today* **2009**, *148*, 350–354.

- (7) Shi, F.; Zhang, Q.; Li, D.; Deng, Y. Silica-Gel-Confined Ionic Liquids: A New Attempt for the Development of Supported Nanoliquid Catalysis. *Chem.—Eur. J.* **2005**, *11*, 5279–5288.

- (8) Xie, Y.; Zhang, Z. F.; Jiang, T.; He, J. L.; Han, B. X.; Wu, T. B.; Ding, K. L.  $\text{CO}_2$  Cycloaddition Reactions Catalyzed by an Ionic Liquid Grafted onto a Highly Cross-Linked Polymer Matrix. *Angew. Chem., Int. Ed.* **2007**, *46*, 7255–7258.

- (9) Dai, W. L.; Chen, L.; Yin, S. F.; Li, W. H.; Zhang, Y. Y.; Luo, S. L.; Au, C. T. High-Efficiency Synthesis of Cyclic Carbonates from Epoxides and  $\text{CO}_2$  over Hydroxyl Ionic Liquid Catalyst Grafted onto Cross-Linked Polymer. *Catal. Lett.* **2010**, *137*, 74–80.

- (10) Udayakumar, S.; Lee, M. K.; Shim, H. L.; Park, D. W. Functionalization of Organic Ions on Hybrid MCM-41 for Cycloaddition Reaction: The Effective Conversion of Carbon Dioxide. *Appl. Catal., A* **2009**, *365*, 88–95.

- (11) Tunckol, M.; Durand, J.; Serp, P. Carbon Nanomaterial-Ionic Liquid Hybrids. *Carbon* **2012**, *50*, 4303–4334.

- (12) Dai, W. L.; Chen, L.; Yin, S. F.; Luo, S. L.; Au, C. T. 3-(2-Hydroxyethyl)-1-propylimidazolium Bromide Immobilized on SBA-15 as Efficient Catalyst for the Synthesis of Cyclic Carbonates via the Coupling of Carbon Dioxide with Epoxides. *Catal. Lett.* **2010**, *135*, 295–304.

- (13) Jutz, F.; Andanson, J. M.; Baiker, A. Ionic Liquids and Dense Carbon Dioxide: A Beneficial Biphasic System for Catalysis. *Chem. Rev.* **2011**, *111*, 322–353.

- (14) Sun, Z. H.; Wang, L. F.; Liu, P. P.; Wang, S. C.; Sun, B.; Jiang, D. Z.; Xiao, F. S. Magnetically Motive Porous Sphere Composite and Its Excellent Properties for the Removal of Pollutants in Water by Adsorption and Desorption Cycles. *Adv. Mater.* **2006**, *18*, 1968–1971.

- (15) Oh, M.; Mirkin, C. A. Chemically Tailorable Colloidal Particles from Infinite Coordination Polymers. *Nature* **2005**, *438*, 651–654.

- (16) Spokoyny, A. M.; Kim, D.; Sumrein, A.; Mirkin, C. A. Infinite Coordination Polymer Nano- and Microparticle Structures. *Chem. Soc. Rev.* **2009**, *38*, 1218–1227.

- (17) Choi, J.; Yang, H. Y.; Kim, H. J.; Son, S. U. Organometallic Hollow Spheres Bearing Bis(N-heterocyclic carbene)-Palladium Species: Catalytic Application in Three-Component Strecker Reactions. *Angew. Chem., Int. Ed.* **2010**, *49*, 7718–7722.

- (18) Park, K. H.; Jang, K.; Son, S. U.; Sweigart, D. A. Self-Supported Organometallic Rhodium Quinonoid Nanocatalysts for Stereoselective Polymerization of Phenylacetylene. *J. Am. Chem. Soc.* **2006**, *128*, 8740–8741.

- (19) Czaja, A. U.; Trukhan, N.; Muller, U. Industrial Applications of Metal-Organic Frameworks. *Chem. Soc. Rev.* **2009**, *38*, 1284–1293.

- (20) Kim, Y.; Choi, Y. S.; Lee, H. J.; Yoon, H.; Kim, Y. K.; Oh, M. Self-Assembly of Fluorescent and Magnetic  $\text{Fe}_3\text{O}_4@C$  Coordination Polymer Nanochains. *Chem. Commun.* **2014**, *50*, 7617–7620.

- (21) Imaz, I.; Hernando, J.; Ruiz-Molina, D.; Maspoch, D. Metal-Organic Spheres as Functional Systems for Guest Encapsulation. *Angew. Chem., Int. Ed.* **2009**, *48*, 2325–2329.

- (22) Liu, D.; Huxford, R. C.; Lin, W. Phosphorescent Nanoscale Coordination Polymers as Contrast Agents for Optical Imaging. *Angew. Chem., Int. Ed.* **2011**, *50*, 3696–3700.

- (23) Lee, H. J.; Cho, W.; Jung, S.; Oh, M. Morphology-Selective Formation and Morphology-Dependent Gas-Adsorption Properties of Coordination Polymer Particles. *Adv. Mater.* **2009**, *21*, 674–677.

- (24) Jeon, Y. M.; Armatas, G. S.; Heo, J.; Kanatzidis, M. G.; Mirkin, C. A. Amorphous Infinite Coordination Polymer Microparticles: A

New Class of Selective Hydrogen Storage Materials. *Adv. Mater.* **2008**, *20*, 2105–2110.

(25) Xu, S.; Liu, J.; Li, D.; Wang, L.; Guo, J.; Wang, C.; Chen, C. Fe-Salphen Complexes from Intracellular pH-triggered Degradation of Fe<sub>3</sub>O<sub>4</sub>@Salphen-In(III) CPPs for Selectively Killing Cancer Cells. *Biomaterials* **2014**, *35*, 1676–1685.

(26) Wei, H.; Li, B.; Du, Y.; Dong, S.; Wang, E. Nucleobase-Metal Hybrid Materials: Preparation of Submicrometer-Scale, Spherical Colloidal Particles of Adenine-Gold(III) via a Supramolecular Hierarchical Self-Assembly Approach. *Chem. Mater.* **2007**, *19*, 2987–2993.

(27) Han, B. Y.; Wang, E. K. Oligonucleotide-Stabilized Fluorescent Silver Nanoclusters for Sensitive Detection of Biothiols in Biological Fluids. *Bioelectron.* **2011**, *26*, 2585–2589.

(28) Xing, L.; Cao, Y.; Che, S. Synthesis of Core-Shell Coordination Polymer Nanoparticles (CPNs) for pH-Responsive Controlled Drug Release. *Chem. Commun.* **2012**, *48*, 5995–5997.

(29) Xing, L.; Zheng, H.; Cao, Y.; Che, S. Coordination Polymer Coated Mesoporous Silica Nanoparticles for pH-Responsive Drug Release. *Adv. Mater.* **2012**, *24*, 6433–6437.

(30) Rieter, W. J.; Pott, K. M.; Taylor, K. M. L.; Lin, W. Nanoscale Coordination Polymers for Platinum-based Anticancer Drug Delivery. *J. Am. Chem. Soc.* **2008**, *130*, 11584–11585.

(31) Imaz, I.; Rubio-Martinez, M.; Garcia-Fernandez, L.; Garcia, F.; Ruiz-Molina, D.; Hernando, J.; Puentes, V.; Maspoch, D. Coordination Polymer Particles as Potential Drug Delivery Systems. *Chem. Commun.* **2010**, *46*, 4737–4739.

(32) Huxford, R. C.; Boyle, W. S.; Liu, D.; Lin, W. Lipid-Coated Nanoscale Coordination Polymers for Targeted Delivery of Antifolates to Cancer Cells. *Chem. Sci.* **2012**, *3*, 198–204.

(33) Xu, S.; You, L.; Zhang, P.; Zhang, Y.; Guo, J.; Wang, C. C. Fe<sub>3</sub>O<sub>4</sub>@Coordination Polymer Microspheres with Self-Supported Polyoxometalates in Shells Exhibiting High-Performance Supercapacitive Energy Storage. *Chem. Commun.* **2013**, *49*, 2427–2429.

(34) Wu, S. S.; Zhang, X. W.; Dai, W. L.; Yin, S. F.; Li, W. S.; Ren, Y. Q.; Au, C. T. ZnBr<sub>2</sub>-Ph<sub>4</sub>PI as Highly Efficient Catalyst for Cyclic Carbonates Synthesis from Terminal Epoxides and Carbon Dioxide. *Appl. Catal., A* **2008**, *341*, 106–111.

(35) Sun, J.; Ren, J. Y.; Zhang, S. J.; Cheng, W. G. Water as an Efficient Medium for the Synthesis of Cyclic Carbonate. *Tetrahedron Lett.* **2009**, *50*, 423–426.

(36) Cui, K. H.; Yao, S. Y.; Li, H. Q.; Li, Y. T.; Zhao, H. P.; Jiang, C. J.; Tian, Y. Q. Acentric and Chiral Four-Connected Metal-Organic Frameworks Based on the Racemic Binaphthol-like Chiral Ligand of 4-(1-H(or methyl)-imidazol-1-yl)benzoic acid. *CrystEngComm* **2011**, *13*, 3432.

(37) Protesescu, L.; Tudorache, M.; Neatu, S.; Grecu, M. N.; Kemnitz, E.; Filip, P.; Parvulescu, V. I.; Coman, S. M. Unusual Behavior of a Novel Heterogeneous Chiral Dimer Cr(III)-Salen Complex in the Epoxidation/Epoxide Ring-Opening Reaction of *trans*-Methylcinnamate Ester. *J. Phys. Chem. C* **2011**, *115*, 1112–1122.

(38) Chang, T.; Jin, L.; Jing, H. Bifunctional Chiral Catalyst for the Synthesis of Chiral Cyclic Carbonates from Carbon Dioxide and Epoxides. *ChemCatChem* **2009**, *1*, 379–383.

(39) An, Q.; Zhang, P.; Li, J. M.; Ma, W. F.; Guo, J.; Hu, J.; Wang, C. C. Silver-Coated Magnetite-Carbon Core-Shell Microspheres as Substrate-Enhanced SERS Probes for Detection of Trace Persistent Organic Pollutants. *Nanoscale* **2012**, *4*, 5210–5216.

(40) An, Q.; Yu, M.; Zhang, Y.; Ma, W.; Guo, J.; Wang, C. C. Fe<sub>3</sub>O<sub>4</sub>@Carbon Microsphere Supported Ag-Au Bimetallic Nanocrystals with the Enhanced Catalytic Activity and Selectivity for the Reduction of Nitroaromatic Compounds. *J. Phys. Chem. C* **2012**, *116*, 22432–22440.

(41) Jo, C.; Lee, H. J.; Oh, M. One-Pot Synthesis of Silica@Coordination Polymer Core-Shell Microspheres with Controlled Shell Thickness. *Adv. Mater.* **2011**, *23*, 1716–1719.

(42) Herreros, B.; Barr, T. L.; Klinowski, J. Spectroscopic Studies of Barium Aluminate Glycolate, Ba[Al<sub>2</sub>(C<sub>3</sub>H<sub>4</sub>O<sub>2</sub>)<sub>4</sub>], A 5-Coordinate Aluminum Compound. *J. Phys. Chem.* **1994**, *98*, 738–741.

(43) Wang, H.; Sun, Y. B.; Chen, Q. W.; Yu, Y. F.; Cheng, K. Synthesis of Carbon-Encapsulated Superparamagnetic Colloidal Nanoparticles with Magnetic-Responsive Photonic Crystal Property. *Dalton Trans.* **2010**, *39*, 9565–9569.

(44) Adamczyk, A.; Dlugon, E. The FTIR Studies of Gels and Thin Films of Al<sub>2</sub>O<sub>3</sub>-TiO<sub>2</sub> and Al<sub>2</sub>O<sub>3</sub>-TiO<sub>2</sub>-SiO<sub>2</sub> Systems. *Spectrochim. Acta, Part A* **2012**, *89*, 11–17.

(45) Caló, V.; Nacci, A.; Monopoli, A.; Fanizzi, A. Cyclic Carbonate Formation from Carbon Dioxide and Oxiranes in Tetrabutylammonium Halides as Solvents and Catalysts. *Org. Lett.* **2002**, *4*, 2561–2563.

(46) Han, L.; Choi, S. J.; Park, M. S.; Lee, S. M.; Kim, Y. J.; Kim, M. I.; Liu, B. Y.; Park, D. W. Carboxylic Acid Functionalized Imidazolium-based Ionic Liquids: Efficient Catalysts for Cycloaddition of CO<sub>2</sub> and Epoxides. *React. Kinet., Mech. Catal.* **2012**, *106*, 25–35.

(47) Pescarmona, P. P.; Taherimehr, M. Challenges in the Catalytic Synthesis of Cyclic and Polymeric Carbonates from Epoxides and CO<sub>2</sub>. *Catal. Sci. Technol.* **2012**, *2*, 2169–2187.